CHAPTER 3

DOSIMETRY OF A 6 MV FFF SMALL PHOTON BEAM USING VARIOUS DETECTORS

This chapter deals with the small-field dosimetry of a 6 MV FFF photon beam using a variety of detectors. These detectors include ionisation chambers, TLDs, diode detectors, and radiochromic films. Small field beam parameters such as output factor, depth dosage, and beam profile of square fields with nominal side lengths of 0.6, 1.0, 2.0, 3.0, 4.0, 5.0, and 6.0 cm were measured and evaluated. The gantry, collimator, and couch angle of LINAC were set to 0^o during small field dosimetry. All of the measurements were carried out in accordance with the procedure established by the International Atomic Energy Agency TRS 483. The results for a variety of dosimetric parameters have been reported in the form of tables and figures in this chapter. Then, these results are compared to the results of other studies that were done in the same way, and a conclusion is drawn.

3.1 INTRODUCTION

Modern medical linear accelerators (LINACs) often utilize high-intensity photon beams for the treatment of small volume tumors. The high intensity or high dose rate mode of treatment delivery is achieved by removal of the flattening filter and is called the unflat or flattening filter-free (FFF) photon beam mode. Compared to flattening filter (FF) beams, the FFF beam results in a 2-4 times higher dose rate, softening of beam quality, dose heterogeneity across the field, reduction in the energy variation across the beam, and a decrease in head scattering (Georg et al., 2011; Ponisch et al., 2006; Cashmore et al., 2008; Dalaryd et al., 2010; Sharma, 2011). Less head scattering may result in reduced leakage and out-of-field dose. FFF photon beams are generally preferred in advanced radiotherapy techniques such as stereotactic radiosurgery, stereotactic radiotherapy, and stereotactic body radiotherapy. These techniques use small radiation fields with high fraction doses for tumor treatment.

The small FFF photon beams deliver the dose precisely and in minimal time in the tumor. This reduces inter-and intra-fractional setup errors and spares normal tissues lying close to the tumor. A precise definition of a small-field in radiation dosimetry is still debatable. A photon beam is frequently defined to have a small-field when the field dimensions are less than the lateral range of the secondary charged particles and there is a partial occlusion of the primary beam source by the collimating device (Bassinet et al., 2013)

The selection of a suitable detector for the accurate measurement of small-fields is more challenging than that for conventional fields. This is more due to the loss of secondary electron equilibrium, partial obstruction of the source, and limitations in the size of the detector. The volume averaging effect can cause dose underestimation and blurring of the penumbra during measurement of small field output factors and beam profiles, respectively (Wuerfel, 2013; Das et al., 2008). A typical way to avoid the volume averaging effect is to select a detector with a very small volume and high spatial resolution. Unlike small-fields of FF beams, those of FFF beam have a higher dose per pulse, enhanced dose rate, and unflat region in the center of the field, which is another measurement-related aspect of the small-field (Wuerfel, 2013).

There are no rules available to guide selection of a specific detector for small-field dose measurements. Therefore, determining the right detector for small-field measurements of FFF beams requires some understanding of the physics of the small-field and a concise idea about the data to be measured. Then, an agreement between all prerequisites must be identified. Several studies of small-field dose measurements with various detectors have been reported, mostly with FF photon beams (Zefkili et al., 1994; Dieterich et al., 2011; Laub et al., 2003; Yang et al., 2003; Yarahmadi et al., 2013; Garcia et al., 2010; Sharma et al., 2017). Therefore, this study aimed to measure the small FFF beam doses using different detectors to increase the available data about the small-field dosimetry of the FFF beams.

The present study aimed to dosimetrically evaluate small-fields of 6 MV FFF photon beams using ionization chambers, thermoluminescent dosimeters (TLDs), diode detectors, and radiochromic films. This study will help in the selection of appropriate detectors to measure the output factors, beam profiles, depth doses, and surface doses of small 6 MV FFF photon beams.

3.2 MATERIALS AND METHODS

3.2.1 Setup used for measurement

Small-field dosimetry of FFF photon beams of LINAC was performed as per the recommendations of the International Atomic Energy Agency (IAEA) code of practice TRS 483 (Palmans et al., 2017). A TrueBeam linear accelerator (Varian

Medical Systems) capable of delivering both FF and FFF photon beams was used. A 6 MV FFF photon beam was used to measure the output factor, depth dose, and beam profile of square fields with nominal side lengths of 0.6, 1.0, 2.0, 3.0, 4.0, 5.0, and 6.0 cm. The gantry, collimator, and couch angle of LINAC were set to 0o during the measurement of beam data. The measurements were performed at a dose rate of 1400 MU/min (monitor unit/minute). The following detectors were used in this study: SNC125c (ionization chamber, Sun Nuclear Corporation), PinPoint (ionization chamber, PTW 31014), EDGE (diode detector, Sun Nuclear Corporation), EBT3 (Gafchromic films, Ashland Advanced Materials), and TLD-100 (TLD chips, Harshaw Chemical Company). The characteristics of the aforementioned detectors are shown in Table 3.1.

The sun nuclear three dimensional (3D) scanner water phantom and PC electrometer were used for beam data measurement (output factor, depth dose, and beam profile) of small-fields. The stems of the SNC125c, PinPoint, and EDGE detectors were oriented perpendicular to the beam central axis in the 3D scanner. The location of the EDGE was indicated by crosshair markings on top of the housing. A high voltage bias of +400V was applied to the SNC125c and PinPoint, as per their calibration certificate indications. No bias voltage was applied to the EDGE. SNC dosimetry software (Sun Nuclear Corporation) was used to analyze the beam data. TLD chips (TLD-100) were utilized to measure the output factors using slabs of a solid water phantom (Sun Nuclear Corporation). The nominal dimensions of the TLD chips were 3.2 mm × 3.2 mm × 0.89 mm. Before each irradiation, the TLD chips were annealed at 400°C for 1 h, followed by a 30 min cool-down period, and 2 h of annealing at 100°C. A Harshaw model 3500 manual TLD reader was used to perform the readout of the TLD chips.

Gafchromic films (EBT3) were used to measure the output factor, depth dose, and profile. The irradiated films were scanned using an Epson Expression 11000XL flatbed scanner. The scan option of a 48 bits color to scan in the RGB (red green blue) mode was selected for film digitization. The spatial resolution selected was 75 dots per inch. Several segments of one sheet of the film were irradiated with doses of 0, 30, 60, 100, 240, 500, and 960 cGy to generate a dose-response calibration curve of the film. The output factors and beam profiles were measured with the EBT3 by placing pieces of the film between the slabs of the solid water phantom at a depth of 10 cm. The percentage depth doses (PDDs) were measured by placing slits of the film between slabs of the solid water phantom in a direction parallel to the beam central axis SNC patient software (Sun Nuclear Corporation) was used to analyze the scanned images.

Table 3.1 Characteristics of the different detectors used in this study.

Feature	SNC125c	PinPoint	EDGE	EBT3	TLD-100
Detector type	Airfilled Ion Chamber	Airfilled Ion Chamber	Shielded Diode	Radiochromic Film	TLD
Make	Sun Nuclear	PTW	Sun Nuclear	Ashland Advanced Materials	Harshaw Chemical Company
Active Volume	0.108 cm^3	0.015 cm^3	0.0019 mm^3	N/A	N/A
Sensitive volume (mm)	Cavity length: 7.05 diameter: 4.75	Cavity length: 5 diameter: 2	Thickness : 0.03 Diameter: 0.8	N/A	N/A
Material	Wall: Graphite Electrode: Aluminium	Wall: Graphite Electrode: Aluminium	Silicon Brass	Active layer based on diacetylene monomers with polyester coating	LiF:Mg,Ti
Effective point	0.6r	0.6r	0.5 mm	Film surface	TLD surface
Water Proof	Yes	Yes	Yes	No	No

3.2.2 Equivalent square small-field size

Nominal small fields were converted to the equivalent square small-field sizes S_{clin} for every field according to the method adopted by TRS 483 using to the following equation:

$$S_{clin} = \sqrt{A.B} \qquad (1)$$

where A and B represent the in-line and cross-line dosimetric field widths, respectively, defined as full-width half maxima (FWHM) at a measurement depth of 10 cm. The dosimetric field widths, A and B, were estimated from the EBT3 measurements.

3.2.3 Output factor measurement

Output factors were measured for nominal square field sizes ranging from 0.6 cm × 0.6 cm to 6.0 cm × 6.0 cm of 6 MV FFF photon beam. Data were taken at 10 cm depth and 90 cm source-to-surface distance in water using SNC125c, PinPoint, EDGE, EBT3, and TLD-100. The dose rate and MU linearity were checked before the output factor measurements and found to be in good agreement with the measured values.

The output factors were calculated from the measured ratio of the detector readings and corrected for the pressure and temperature of each ionization chamber. The output factor measurements presented for each detector were normalized to their corresponding values for calibration reference field of 10 cm × 10 cm. The variation between the output factors obtained with the different detectors and those obtained from the EBT3 film was estimated.

Simultaneously, the output factors were also derived for ion chambers and diodes from the measured ratio of detector readings multiplied by an output correction factor recommended elsewhere (Palmans et al., 2017; Tanny et al., 2015). This converted the ratio of measured readings into the ratio of the absorbed dose to water for the PinPoint and EDGE. Volume averaging was not negligible for the smallest fields measured using TLD-100. Therefore, the output factors obtained from TLDs

were multiplied by the volume-averaging correction factor reported in an earlier study (Azangwe et al., 2014). Additionally, we estimated the output correction factor for SNC125c by calculating the direct ratios of the mean of the output factors of a particular field size obtained from the above four detectors to that of SNC125c.

The output factors in terms of the absorbed dose to water for small-fields were calculated using the method discussed in TRS 483 in the following way:

$$\Omega_{Q_{clin}Q_{msr}}^{f_{clin}f_{msr}} = \frac{M_{Q_{clin}}^{f_{clin}}}{M_{Q_{msr}}^{f_{msr}}} k_{Q_{clin}Q_{msr}}^{f_{clin}f_{msr}} \qquad (2)$$

3.2.4 Estimation of experimental uncertainties

To estimate the experimental uncertainties associated with the measurement of output factors using different detectors, we adopted a methodology similar to that described in earlier studies (Francescon et al., 2011; IAEA 2008). In short, we performed four sessions of measurement for each detector over two months, with one session regularly every two weeks. Each session has three sub sessions of measurement. In between every sub sessions, the experimental setup condition was re-setup in such a way that if it is a new day for measurement. The output factors were measured using three active detectors (SNC125c, PinPoint, and EDGE) and two passive detectors (EBT3 and TLD-100). Each measurement of output factor was averaged over a series of at least four repeated meter-readings for active detectors and four times read-out for passive detectors. In the case of an active detector, the position of the detector was realigned based on measurement of profiles for the smallest field. This method estimates the overall experimental uncertainty associated with the measurement of output factor mainly due to dosimeter positioning induced error, misalignment of phantom, uncertainty in setting the source-to-surface distance with the optical distance indicator, displacement of beam central axis, and output fluctuation of a LINAC. The combined standard uncertainty was assessed using the method described in IAEA TECDOC 1585 (IAEA 2008).

To obtain the overall standard uncertainty for the output factors $\Omega_{Q_{clin}Q_{msr}}^{f_{clin}f_{msr}}$ obtained from ion chambers and diodes, the experimental uncertainties were

combined with the uncertainty of the output correction factors $k_{Q_{clin}Q_{msr}}^{f_{clin}f_{msr}}$ given in Table 37 of IAEA TRS 483.

3.2.5 Beam profile and PDD measurement

In this study, cross-line beam profiles and PDDs of field sizes between 0.6 cm × 0.6 cm and 6.0 cm × 6.0 cm of 6 MV FFF photon beams were measured in water using an EDGE, EBT3, SNC125c, and PinPoint. The cross-line profiles were measured at a depth of 10 cm in a source to axis setup, and PDD curves were obtained by moving the dosimeter along the direction of the beam central axis. The measured beam profiles were re-scaled as suggested by an earlier study (Ponisch et al., 2006) therefore, the penumbra definition of FF photon beams could be applied to FFF photon beams. After re-scaling, the penumbra of the FFF beam was defined as the lateral distance between the 20% and 80% dose levels in the field. The left and the right penumbra of each small field were estimated using cross-line profiles, and the average value of the penumbra was reported. FWHM values were also calculated after renormalization of the profiles at the central axis. The degree of unflatness (DOU), as per Eq. (3), was defined as the ratio of the dose level at the beam central axis and the dose level at the predefined off-axis of a beam profile (Georg et al., 2011; Fogliata et al.,2012).

Here, the predefined off-axis of a beam profile was the distance from the beam central axis as a function of field size and was selected as 60% of the field size for field-side < 10 cm.

$$DOU = \frac{Dose_{Beamcentralaxis}}{Dose_{Predefinedoff-axis}} \qquad (3)$$

The definition of symmetry for FFF and FF beams differed only in the evaluation area, which was to be within the field region for FFF beams and within the flat region for FF beams (Fogliata et al., 2012).

The percentage surface dose (DS), PDD at 10 cm (D10), and depth of maximum dose (dmax) were evaluated from the PDD scans and reported. The surface dose parameter DS was defined as the relative dose at a depth of 0.5 mm to the dose at dmax. The beam profile and PDDs of 6 MV FFF beam measured using different detectors are shown in the Figure 3.1-3.6 and 3.7-3.12, respectively.

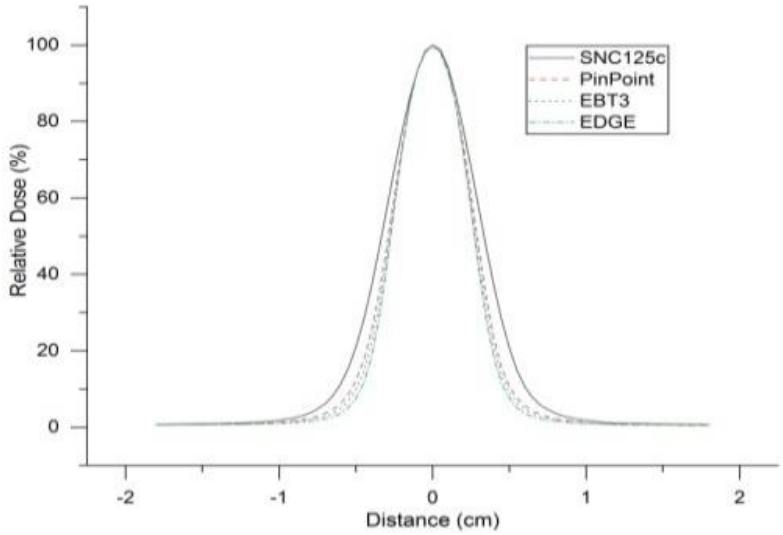

Figure 3.1 Beam profiles of 6 MV flattening filter-free (FFF) beam measured using different detectors for field size 0.6 cm × 0.6 cm.

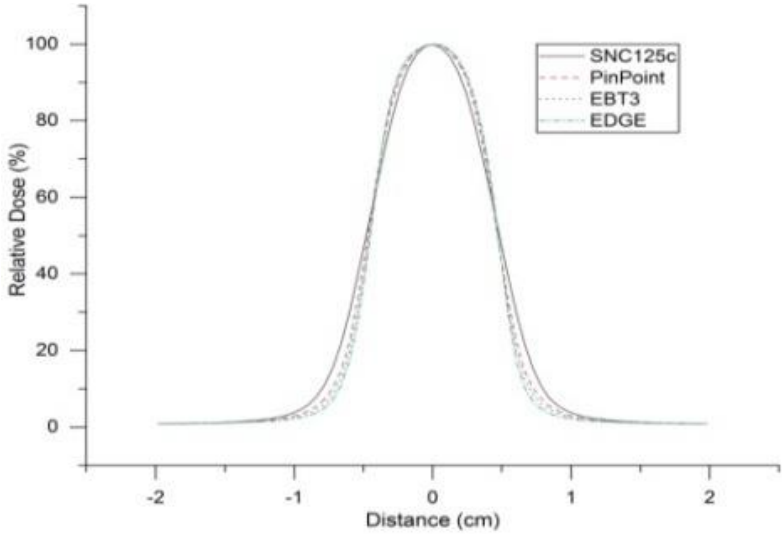

Figure 3.2 Beam profiles of 6 MV flattening filter-free (FFF) beam measured using different detectors for field size 1.0 cm × 1.0 cm.

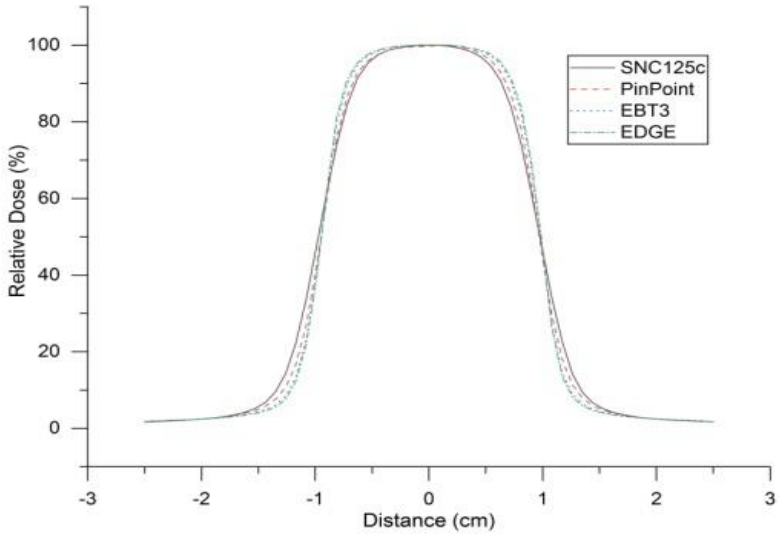

Figure 3.3 Beam profiles of 6 MV flattening filter-free (FFF) beam measured using different detectors for field size 2 cm × 2 cm.

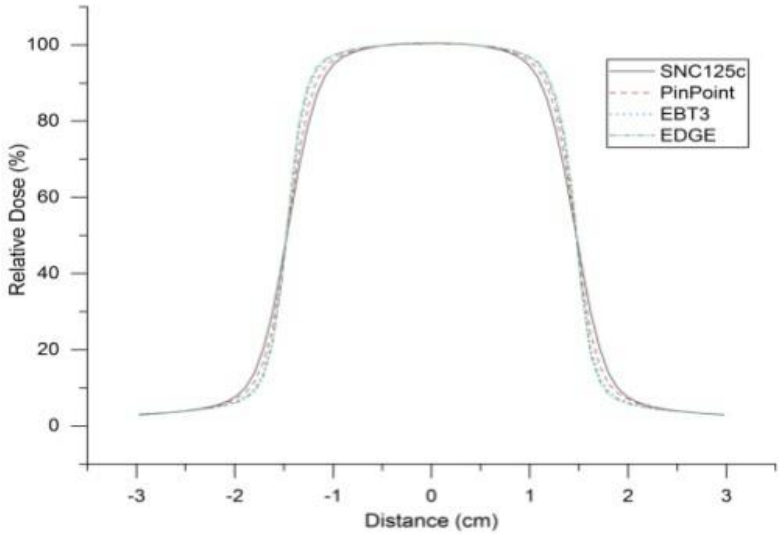

Figure 3.4 Beam profiles of 6 MV flattening filter-free (FFF) beam measured using different detectors for field size 3 cm × 3 cm.

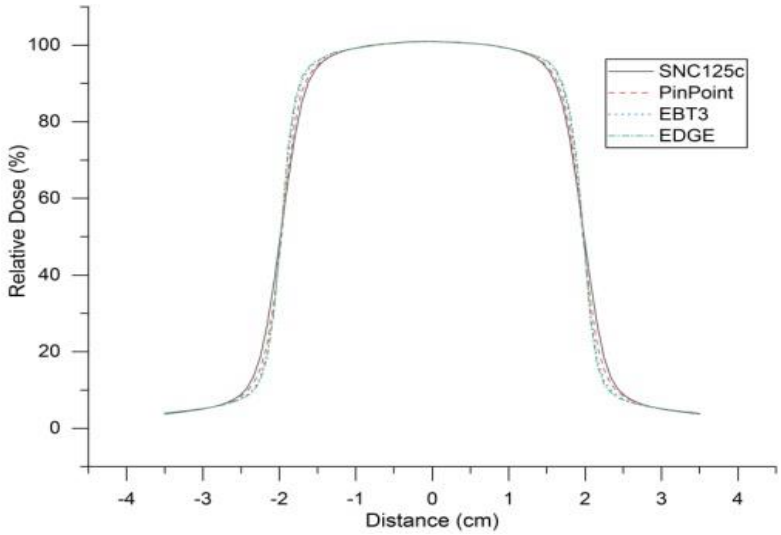

Figure 3.5 Beam profiles of 6 MV flattening filter-free (FFF) beam measured using different detectors for field size 4 cm × 4 cm.

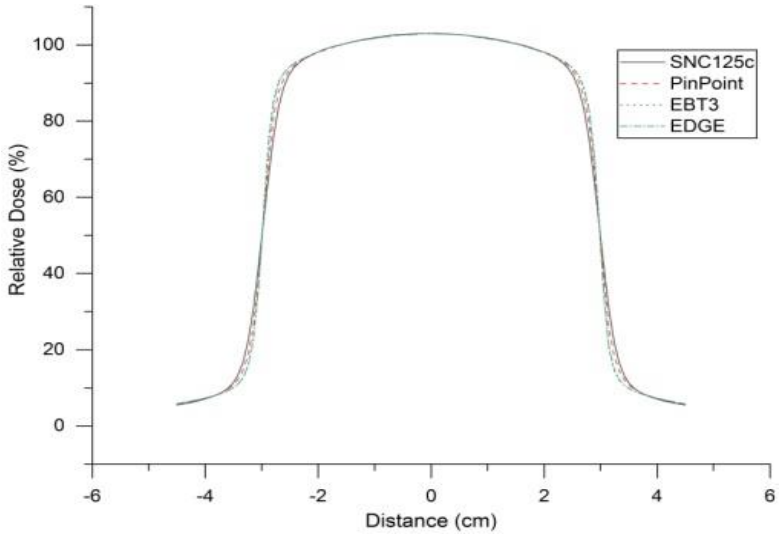

Figure 3.6 Beam profiles of 6 MV flattening filter-free (FFF) beam measured using different detectors for field size 6 cm × 6 cm.

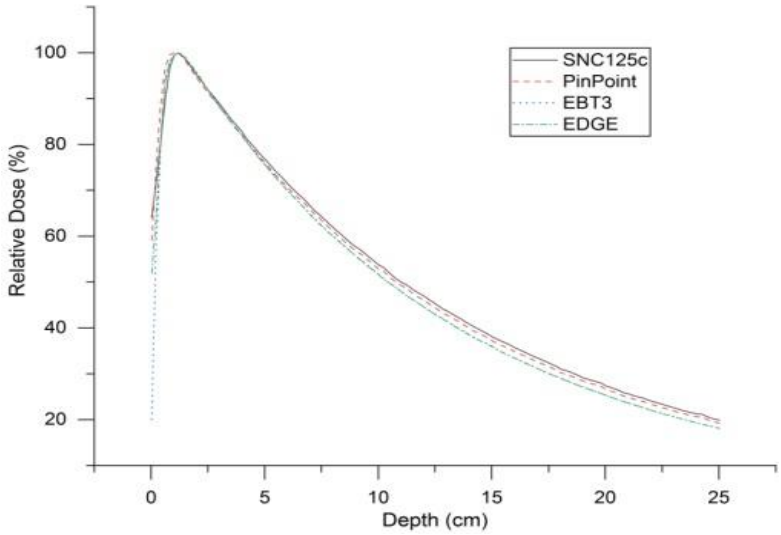

Figure 3.7 Percentage depth doses (PDDs) of 6 MV flattening filter-free (FFF) beam measured using different detectors for field size 0.6 cm × 0.6 cm.

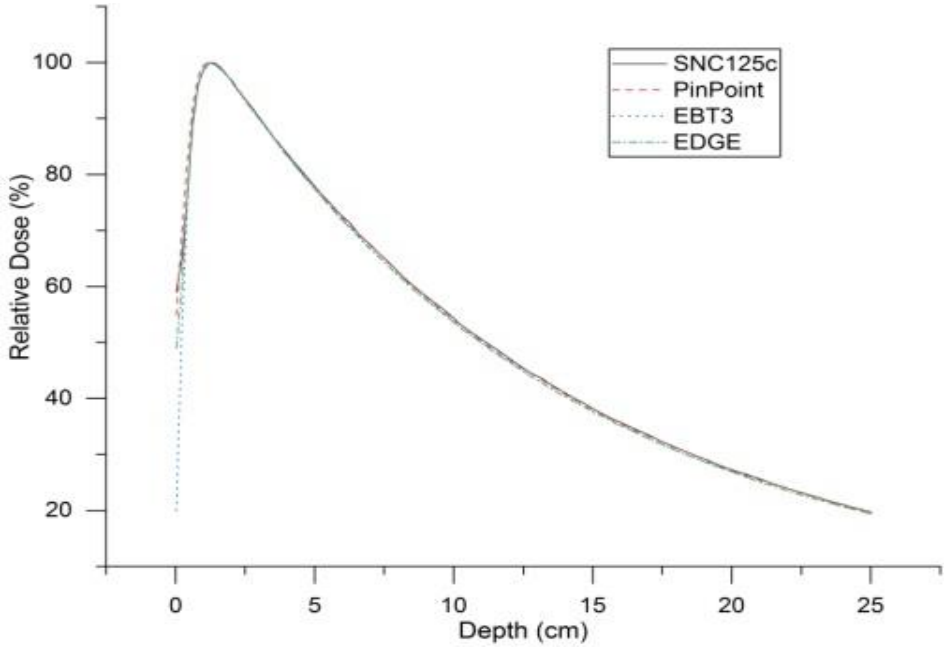

Figure 3.8 Percentage depth doses (PDDs) of 6 MV flattening filter-free (FFF) beam measured using different detectors for field size 1 cm × 1 cm.

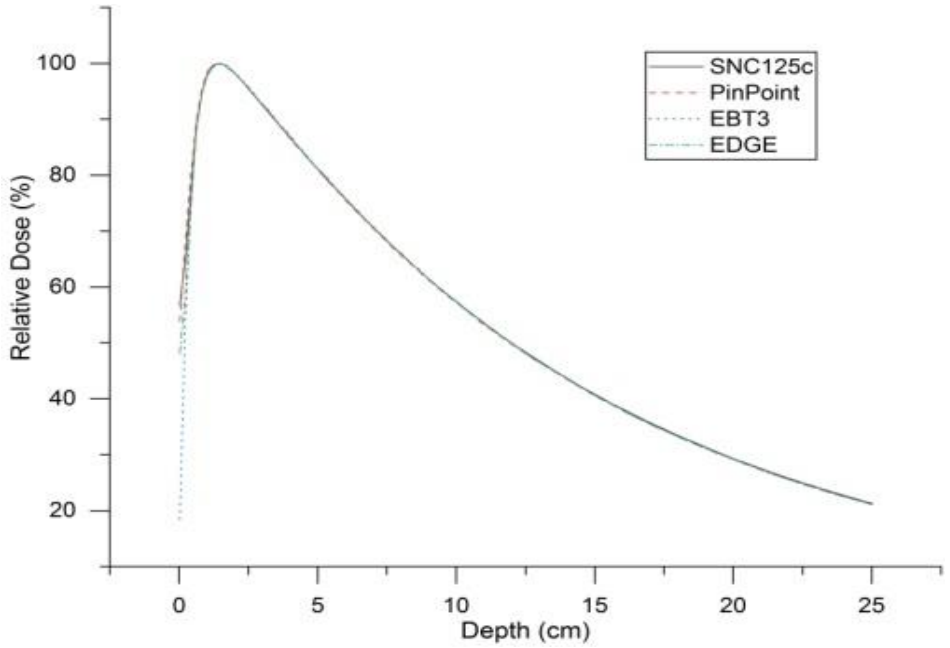

Figure 3.9 Percentage depth doses (PDDs) of 6 MV flattening filter-free (FFF) beam measured using different detectors for field size 2 cm × 2 cm.

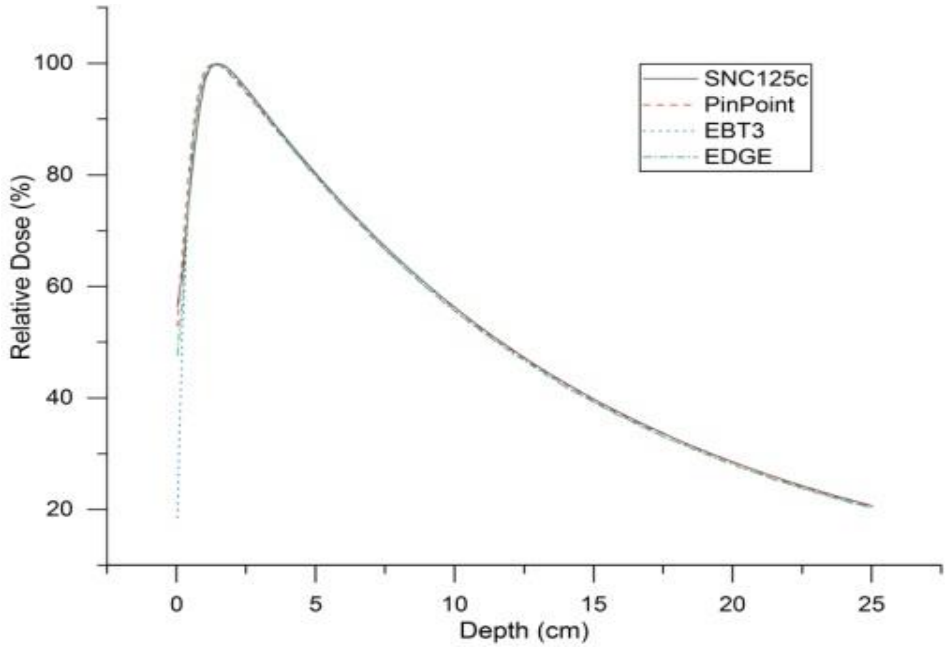

Figure 3.10 Percentage depth doses (PDDs) of 6 MV flattening filter-free (FFF) beam measured using different detectors for field size 3 cm × 3 cm.

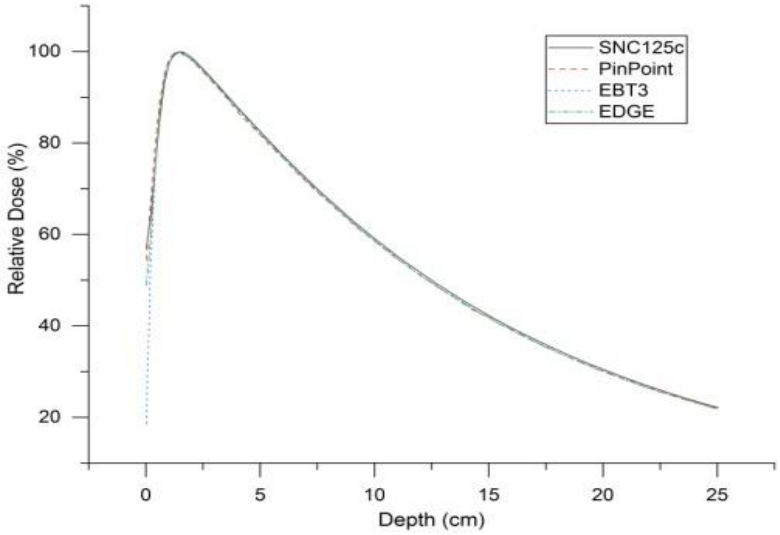

Figure 3.11 Percentage depth doses (PDDs) of 6 MV flattening filter-free (FFF) beam measured using different detectors for field size 4 cm × 4 cm.

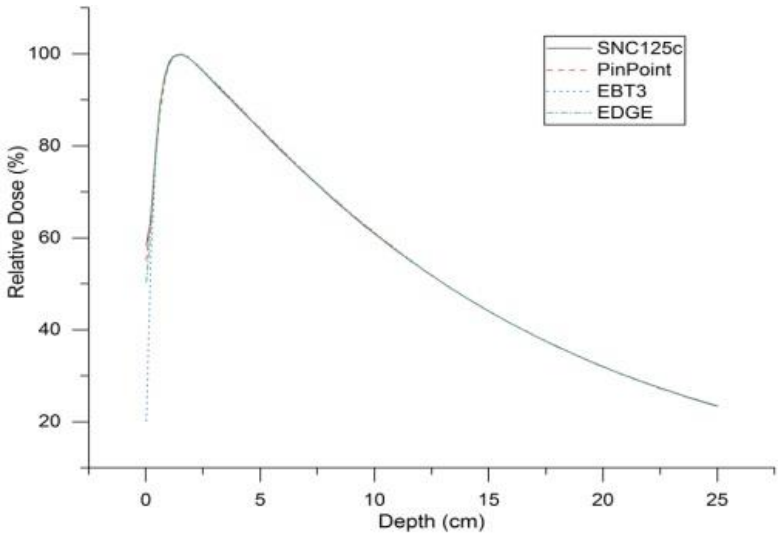

Figure 3.12 Percentage depth doses (PDDs) of 6 MV flattening filter-free (FFF) beam measured using different detectors for field size 6 cm × 6 cm.

3.3 RESULTS

3.3.1 Equivalent square small field size S_{clin}

For every nominal field, the corresponding equivalent square small-field sizes (S_{clin}) were estimated according to Eq. (1). The results for the nominal and equivalent square small-field sizes are presented in Table 3.2. In this study, the field sizes are expressed with nominal values only; however, invariably, they correspond to the respective S_{clin}.

Table 3.2 Nominal square field sizes and corresponding equivalent square small field sizes for 6 MV flattening filter-free (FFF) beams of Varian TrueBeam linear accelerator.

Nominal square field size (cm)	Equivalent square small field size, S_{clin} (cm)
0.6	0.63
1.0	1.01
2.0	2.00
3.0	2.99
4.0	4.02
5.0	5.01
6.0	5.98
10.0	9.95

3.3.2 Output factor

The output factors of different detectors estimated directly from the ratio of detector readings for field sizes between 0.6 cm × 0.6 cm and 6 cm × 6 cm are plotted in Figure 3.13. The detector-to-detector variation in the output factors for field sizes between 2 cm× 2 cm and 6 cm× 6 cm was found to be within 1%, with a relative standard deviation (RSD) of less than 0.70%. The difference in the output factors for the remaining field sizes was significant. Compared to the EBT3, the SNC125c, PinPoint, TLD-100, and EDGE showed variations of -25.38%, -6.95%, -4.32%, and

2.63% for the field size of 0.6 cm × 0.6 cm (RSD of 11.83%) and -5.67%, -3.40%, -1.56%, and 1.70% for field size of 1.0 cm × 1.0 cm (RSD of 2.93%), respectively.

This ratio of detector readings was generally considered as the output factor before the publication of the TRS 483 code of practice (COP). This COP highlights that deriving the output factor for small-fields directly from the quotient of detector readings is incorrect because $k_{Q_{clin}Q_{msr}}^{f_{clin}f_{msr}}$ is unknown. Therefore, the output correction factors recommended by earlier studies (Palmans et al., 2017; Tanny et al., 2015) were applied to the measured ratio of detector readings for PinPoint and EDGE according to Eq. (2). The estimated correction factors of SNC125c for nominal square fields of length 0.6cm, 1.0 cm, 2.0 cm, 3.0 cm, 4.0 cm, 5.0 cm, and 6.0 cm were 1.335, 1.055, 1.009, 0.999, 0.997, 0.996, and 1.001, respectively. For the smallest field (0.6 cm × 0.6 cm), detectors such as EDGE, PinPoint,and SNC125c exhibited the largest corrections of -5.1%, 10.3%, and 33.5%, respectively, to their readings. The reported volume averaging correction factors of TLD-100 for the 0.6, 1.0, and 2 cm square field sides are 1.029, 1.005, and 1.001, respectively, while it was unity for the remaining fields. The corrected output factors derived after applying these corrections are plotted in Figure 3.14. The differences in the corrected output factors measured using the SNC125c, PinPoint, TLD-100, and EDGE relative to that obtained with EBT3 are -0.36%, 2.63%, -1.50%, and -2.60% for a field size of 0.6 cm × 0.6 cm (RSD of 1.97%) and -0.49%, -0.95%, -1.13%, and -1.76% for 1.0 cm × 1.0 cm, respectively (RSD of 1.05%), whereas the variations in the remaining fields were found to be within 1% (RSD less than 0.30%).

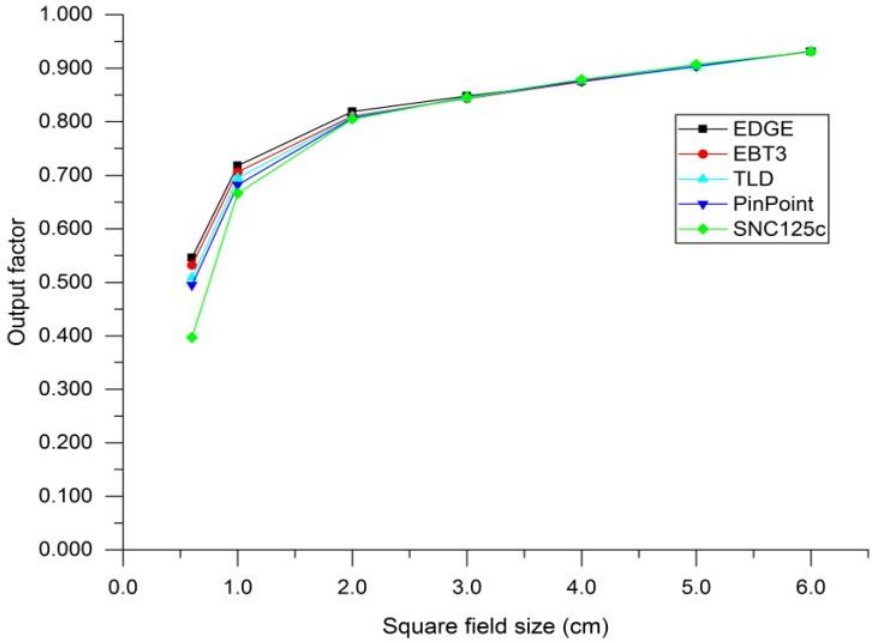

Figure 3.13 Output factor (without corrections) of a 6 MV flattening filter-free (FFF) beam as a function of field size measured using different detectors.

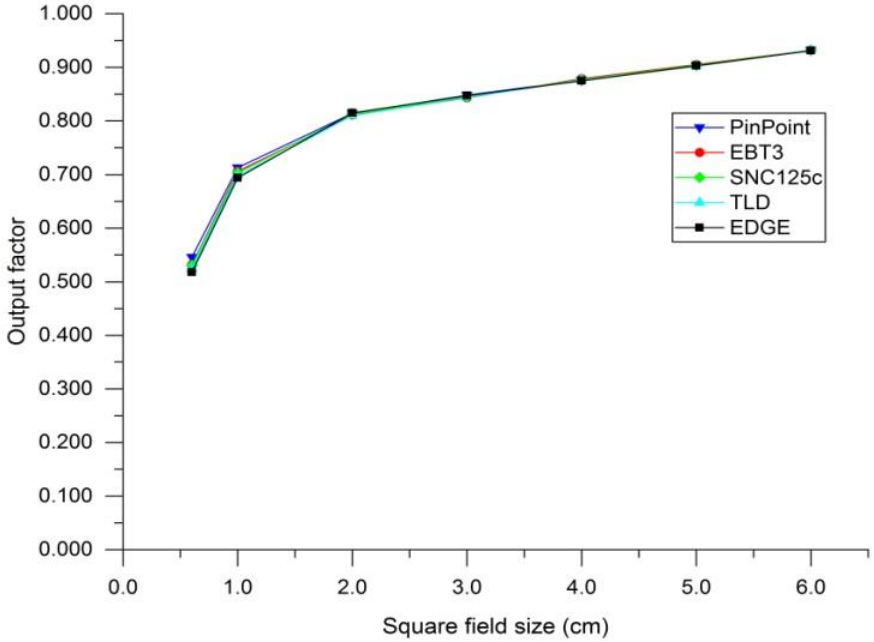

Figure 3.14 Output factor (with corrections) of 6 MV flattening filter-free (FFF) beam as a function of field size measured using different detectors.

The overall standard uncertainties associated with various detectors for each nominal square field size are listed in Table 3.3. The estimated measurement uncertainty is based on a standard uncertainty multiplied by a coverage factor k = 2, which provided an uncertainty of two standard deviations and an approximately 95% confidence level (CI). The calculated uncertainty (k = 2, 95% CI) was highest for SNC125c, with an average value at 2.7%, and for EDGE at 0.9% (lowest).

Table 3.3 Overall standard uncertainty (*k* = 2, 95% confidence interval [CI]) evaluated for different detectors.

Square field size (cm)	SNC125c	PinPoint	EDGE	EBT3	TLD-100
0.6	8.7	5.1	1.5	4.8	4.6
1.0	5.1	2.3	1.1	3.4	2.6
2.0	1.5	1.0	0.9	2.5	1.4
3.0	1.0	0.9	0.8	2.1	1.2
4.0	0.9	0.8	0.6	1.9	1.0
5.0	0.9	0.9	0.6	1.7	1.0
6.0	0.6	0.6	0.6	1 .7	0.8

3.3.3 Beam profile

Figure 3.1-3.6 shows the cross-line profiles of the small fields measured using different detectors, renormalized to the beam central axis as suggested by a previous study (Ponisch et. al., 2006). The profiles show differences at the edges of the beam, the profiles of EDGE measurements were much steeper than those of other detectors. EBT3 and EDGE exhibit nearly identical profiles. The steep changes in the slope of the profiles measured with SNC125c were smoothed slightly than with PinPoint.

3.3.3.1 FWHM

The results of the FWHM are shown in Figure 3.15. On comparison of each set of FWHM measured using different detectors with EBT3, the maximum variation was found to be within 1.0 mm, 0.4 mm, 0.4 mm, 0.2 mm, 0.3 mm, 0.1 mm, and 0.1 mm for 0.6 cm × 0.6 cm, 1.0 cm × 1.0 cm, 2.0 cm × 2.0 cm, 3.0 cm × 3.0 cm, 4.0 cm × 4.0 cm, 5.0 cm × 5.0 cm, and 6.0 cm × 6.0 cm nominal square fields, respectively. Compared to EBT3, the beam profile measured with the SNC125c showed the maximum difference of 1 mm in FWHM at a field size of 0.6 cm × 0.6 cm.

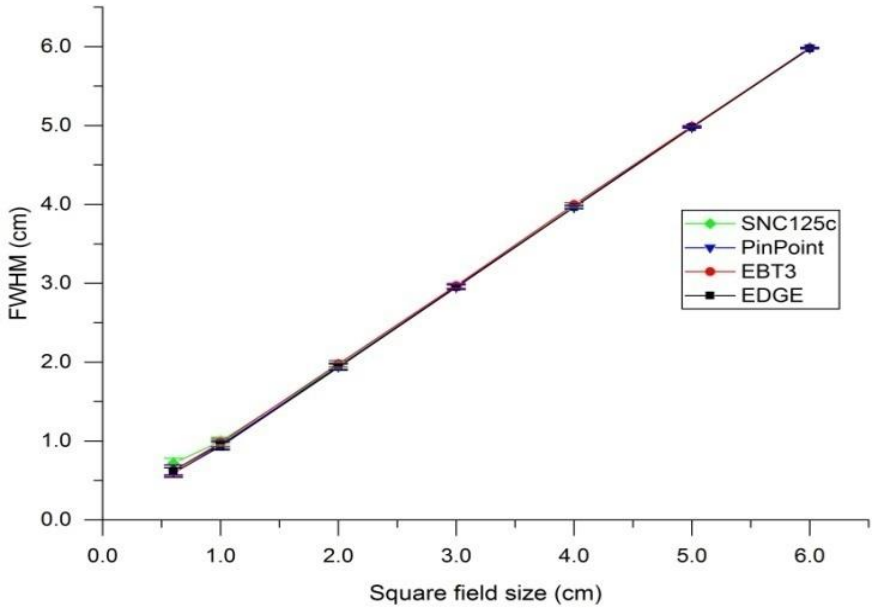

Figure 3.15 Full-width half maxima (FWHM) of 6 MV flattening filter-free (FFF) beam as a function of field size measured using different detectors.

3.3.3.2 Radiation beam penumbra (d20-80)

The $d_{20\text{-}80}$ findings for different detectors as a function of field size are plotted in Figure 3.16. The beam profile measured with the SNC125c showed the largest penumbra for all field sizes, whereas the smallest was recorded by the EDGE. The maximum difference between these two detectors was 1.80 mm for 6 cm × 6 cm field size and the minimum was 0.98 mm for 0.6 cm × 0.6 cm. Penumbra measurement from EBT3 and EDGE was found to be in a very close agreement for all field sizes and the maximum variation between the two detectors was 0.14 mm for the field size

of 0.6 cm × 0.6 cm. Maximum and minimum penumbra variation between PinPoint and EDGE was 0.75 mm and 0.31 mm for 6 cm × 6 cm and 0.6 cm × 0.6 cm field sizes, respectively.

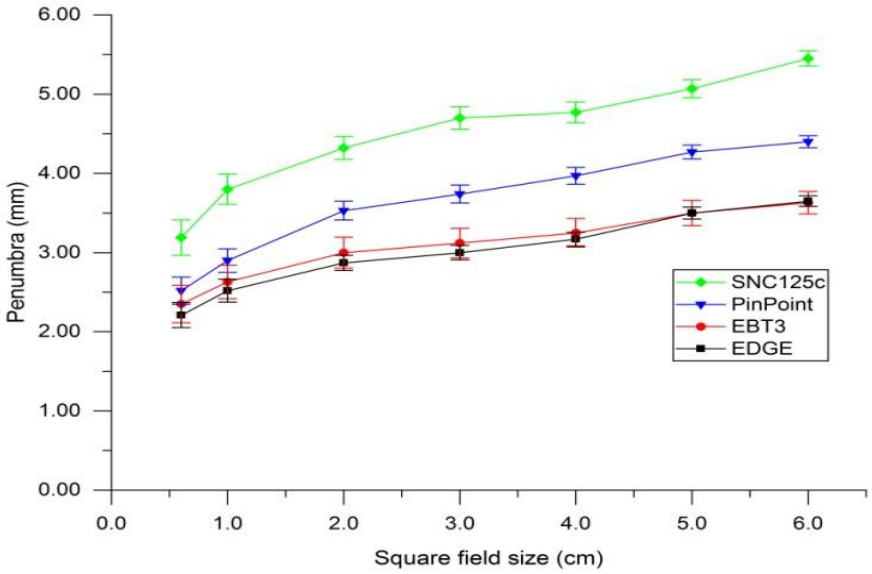

Figure 3.16 Penumbra of 6 MV flattening filter-free (FFF) beam as a function of field size measured using different detectors.

3.3.3.3 Degree of unflatness

The findings of degree of unflatness are shown in Figure 3.17. The unflatness for a field size of 2 cm × 2 cm to 6 cm × 6 cm was found to be in the range of 1.030–1.079 for SNC125c; 1.030–1.061 for PinPoint; 1.026–1.038 for EBT3, and 1.025–1.036 for EDGE. The values of unflatness were 1.255 for SNC125c; 1.194 for PinPoint; 1.161 for EBT3 and 1.157 for EDGE for field size of 1 cm × 1 cm and 1.24 for SNC125c; 1.27 for PinPoint; 1.30 for EBT3 and 1.29 for EDGE for field size of 0.6 cm × 0.6 cm.

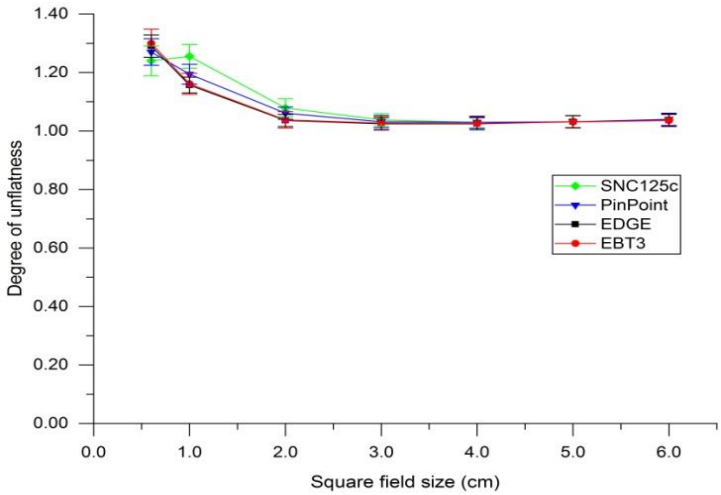

Figure 3.17 Degree of unflatness of 6 MV flattening filter-free (FFF) beam as a function of field size measured using different detectors.

3.3.3.4 Beam symmetry

The symmetry results are presented in Figure 3.18. The percentage symmetry measured with all the detectors for field sizes of 0.6 cm × 0.6 cm to 6 cm × 6 cm was found to be within 100% to 101%.

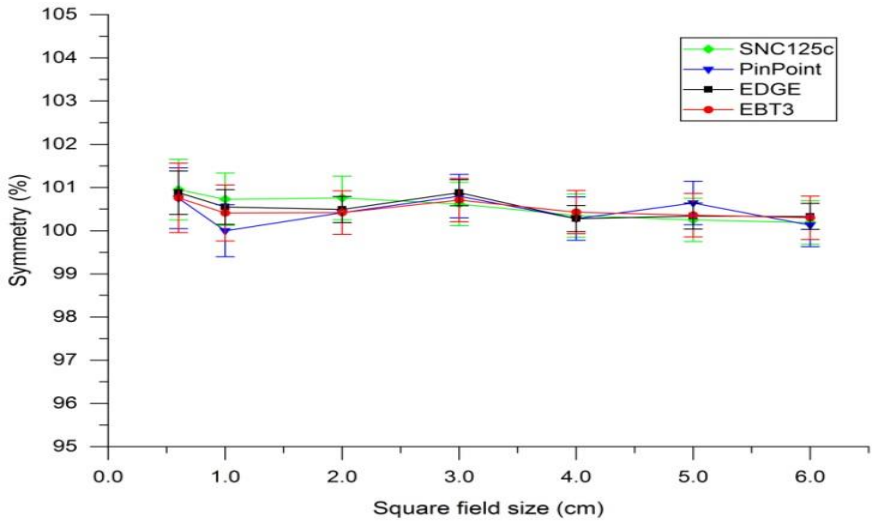

Figure 3.18 Symmetry of 6 MV flattening filter-free (FFF) beam as a function of field size measured using different detectors.

3.3.4 Depth dose

Figure 3.7 to 3.12 shows the PDD curves of the small fields measured using different detectors. Detector-to-detector variation of the PDD data points was

significant up to a depth of 1 cm in the build-up area. While almost all the data were within 1% at depths greater than 1 cm, except for a field size of 0.6 cm × 0.6 cm, where SNC125c had variations of more than 1% and the maximum variation was of 2.5%.

3.3.4.1 Percentage surfaces dose (D_S)

The percentage surface doses are shown in Figure 3.19. The maximum variation in the surface dose for the smallest field size (≤ 1 cm × 1 cm) was 3.69% between SNC125c and PinPoint, 7.68% between PinPoint and EDGE, and 27.69% between EDGE and EBT3. The maximum variation in the surface dose for field sizes from 2 cm × 2 cm to 6 cm × 6 cm was 1.95% between SNC125c and PinPoint, 5.97% between PinPoint and EDGE, and 26.73% between EDGE and EBT3. Compared with that obtained with film measurement, the surface dose was found to be much higher in all the other detectors.

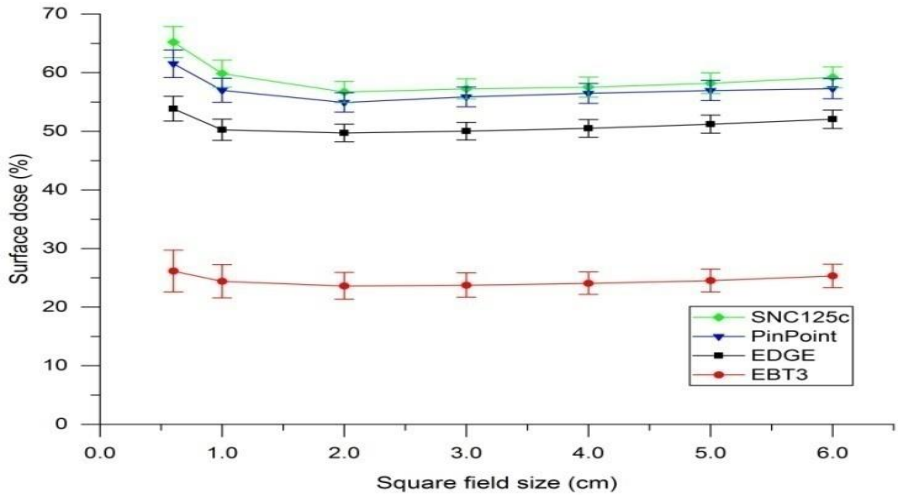

Figure 3.19 Surface dose of 6 MV flattening filter-free (FFF) beam as a function of field size measured using different detectors.

3.3.4.2 Percentage depth dose at 10 cm (D_{10})

The values of D_{10} observed with various detectors for field sizes between 0.6 cm × 0.6 cm and 6 cm × 6 cm are plotted in Figure 3.20. The detector-to-detector variation in the D_{10} between 1 cm × 1 cm and 6 cm × 6 cm field sizes was minimal, with a 1 cm × 1 cm yielding a maximum variation of 1.34% (RSD = 0.62%). The remaining field size (0.6 cm × 0.6 cm) differed by ≤ 4%, with an RSD of 1.80%.

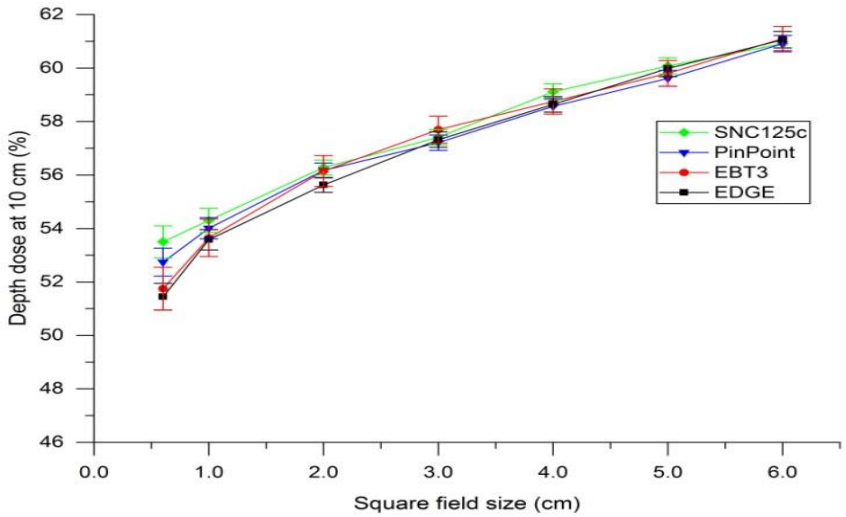

Figure 3.20 Depth dose of 6 MV flattening filter-free (FFF) beam as a function of field size measured using different detectors.

3.3.4.3 Depth of maximum dose (d_{max})

The values of d_{max} measured with various detectors for field sizes between 0.6 cm × 0.6 cm and 6 cm × 6 cm are shown in Figure 3.21. The d_{max} observed with various detectors were ranging between 12.0–12.1 mm for a field size of 0.6 cm × 0.6 cm, 12.5–12.7 mm for 1 cm × 1 cm, 14.0–15.0 mm for 2 cm × 2 cm, and 15.0–15.2 mm for all other field sizes.

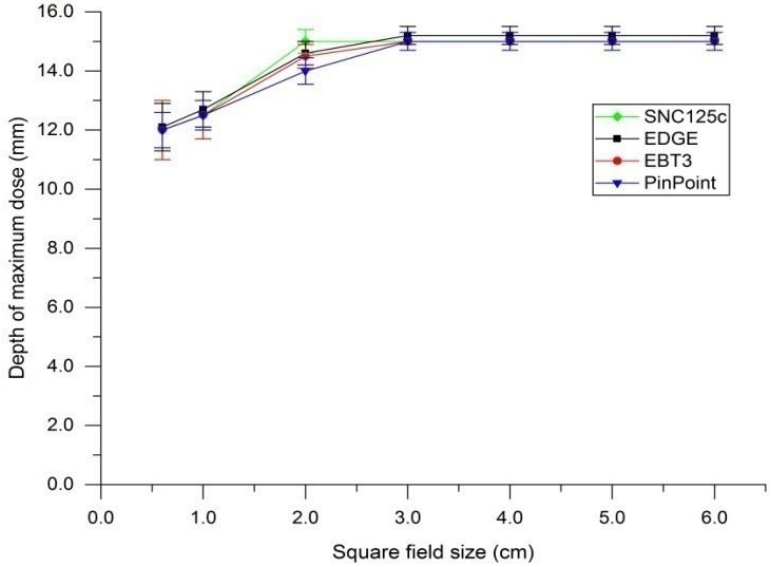

Figure 3.21 Depth of maximum dose of 6 MV flattening filter-free (FFF) beam as a function of field size measured using different detectors.

3.4 DISCUSSION

In this study, we determined the output factors of small-fields according to TRS 483 along with their measurement uncertainties. For comparison, we first estimated the output factors, as traditionally performed by users in the absence of TRS 483 correction factors. The output factors estimated as the ratio of detector readings with SNC125c, PinPoint, TLD-100, EBT3, and EDGE for field sizes between 2 cm × 2 cm and 6 cm × 6 cm were found to be in good agreement (RSD < 0.70%). The remaining field sizes 0.6 cm × 0.6 cm and 1.0 cm × 1.0 cm showed significant variation with RSD of 11.83% and 2.93%, respectively. For field sizes ≤ 1 cm × 1 cm, air-filled ionization chambers recorded the minimum values of the output factor with decreasing field sizes, which is due to the volume averaging effect associated with ionization chambers (Laub et at., 2003). As illustrated in Figure 3.13, the SNC125c showed the lowest value of the output factor for the smallest field size (≤ 1 cm × 1 cm), while the largest value was recorded by the EDGE detector, and the difference between the two values was the highest. Compared to that with the SNC125c, the output factors measured with the PinPoint showed a higher value for the smallest fields (≤ 1 cm × 1 cm). This is owing to the fact that the volume of the PinPoint is nearly eight times smaller than that of the SNC125c (Pappas et al., 2006). Moreover, the EDGE measured the largest value of the output factor due to the density of its material (silicon), which is higher than that of water (Westermark et al., 2000) and the sensitivity of diodes is higher than that of the ionization chambers.

We found that after applying the correction factors suggested by published studies (Palmans et al., 2017; Tanny et al., 2015; Azangwe et al., 2014; Huq et al., 2018; Tyler et al., 2016; Underwood et al., 2015) to our measurements, the smallest fields 0.6 cm × 0.6 cm and 1.0 cm × 1.0 cm showed minimal variation with RSD of 1.97% and 1.05%, respectively, and remaining fields were found to be in good agreement with RSD of less than 0.30%. On comparison of each set of corrected output factors measured using different detectors with EBT3, the variation was found to be within 3.0%, 2.0%, and 1.0% for 6 cm × 0.6 cm, 1.0 cm × 1.0 cm, and remaining nominal square fields, respectively. Furthermore, each set of corrected output factors was compatible with almost every other when the experimental uncertainty was considered. The accurate response of EBT3 for small-field dosimetry is due to its high spatial resolution, tissue equivalence, and low energy dependence (Garcia et al.,

2010). Output factor measurement using TLDs provide excellent results owing to their high spatial resolution and dose-response (Pappas et al., 2006). The measurement of output factors with all the above mentioned detectors agree with previously published data (Dalaryd et al.,2010; Bassinet et al., 2013; Wuerfel 2013; Das et al., 2008; Zhang et al., 2015; Akino et al., 2020; Casar et al., 2019; Lechner et al., 2013). The form of the overall standard uncertainty observed for different fields and detectors is similar to that in other publications, although the values are not directly relatable owing to differences in the beam shaping device, field sizes, and methodology used in other studies (Bassinet et al., 2013; Francescon et al., 2011; Cranmer et al., 2011; Ralston et al., 2012). In general, standard uncertainty decreased with an increase in the radiation field size.

The beam profiles measured with EDGE and EBT3 were much steeper at the edges of the beam compared to ionization chambers, due to their high spatial resolution in the gradient region of the profile. EBT3 measurements did not achieve as high a spatial resolution as an EDGE, which may be due to the higher noise contribution for small fields. Ionization chambers have a volume averaging effect due to their finite size, leading to even lower spatial resolution, especially in the large gradient region of the dose profile. Generally, the spatial resolution of a dosimeter depends inversely on its active volume. We evaluated the profiles for small fields and found a variation of less than 0.5 mm in the FWHM values between different detectors and EBT3, except that SNC125c showed the largest variation of 1 mm for the smallest field (0.6 cm × 0.6 cm). This is due to the relatively large volume of the SNC125c ion chamber compared to the size of the radiation field, which results in the effect of volume averaging. Similar results have been reported previously (Akino et al., 2020; Hsueh et al., 2019).

In small-field dosimetry, accurate measurement of the penumbra is important owing to the increased curvature in the penumbra region (Wuerfel 2013). A significant difference in penumbra was observed between various detectors, which has also been reported in another study (Chang et al., 1996). The beam profiles of the small field measured using the EBT3 and EDGE showed the smallest penumbra, and the difference between the two detectors was negligible. The PinPoint showed a penumbra approximately 1 mm less than that of the SNC125c, which is due to the active volume of the former being eight times smaller than that of the latter (Laub et

al., 2003; Azangwe et al., 2014). Among the different dosimeters used in this study, the SNC125c showed a broadened penumbra, whereas the EDGE recorded the narrowest. This study found that ion chambers overestimated the measured penumbra, while EDGE and EBT3 accurately estimated penumbra. These results are in agreement with the data obtained from other published studies (Akino et al., 2020; Hsueh et. al., 2019; Chang et al., 1996; Bucciolini et al., 2003; Gonzalez et al., 2015; Monasor et al., 2019). The enlarged penumbra observed with ionization chambers was due to a higher range of secondary electrons being present in air than in water and the volume averaging effect. However, the narrowest penumbra was obtained with the EDGE as the change in electron transport from silicon to water was quite low. The EBT3 and EDGE were found to be suitable for the measurement of doses in high-dose gradient regions (such as penumbra) due to their high spatial resolution.

The beam profile of the FFF photon beam is always un-flat in the center of the radiation beam. The beam profile measured with the EBT3 and EDGE showed the lowest degree of unflatness, while the SNC125c exhibited the highest degree of unflatness. The PinPoint findings showed a reasonable difference with those obtained with EBT3 and EDGE for the field sizes below 2 cm × 2 cm, whereas the latter two detectors showed a close agreement for degree of unflatness for all field sizes. The results of this study showed that a 6 MV FFF beam was almost flat for field sizes between 3 cm × 3 cm and 4 cm × 4 cm. The unflatness increased slightly for field sizes above 4 cm × 4 cm and significantly for those below 2 cm × 2 cm for all detectors. Ionization chambers showed a dip in the unflatness for a field size of 0.6 cm × 0.6 cm, and the dip was more pronounced with the increasing volume of the ion chamber. This may be owing to the volume effect and noticeable difference in electron transport from air to water for different chambers. The beam symmetry was also analyzed using various detectors and showed no variation for all small-field sizes. These results are consistent with data reported in the literature (Fogliata et al., 2012; Kehwar et al., 2006).

The spectrum of the FFF photon beam is relatively softer than that of the FF photon beam owing to the loss of beam hardening occurring through the flattening filter (Georg et al., 2011; Sahani et al., 2014). This may enhance the surface dose in the case of FFF photon beams. Detector to detector comparison was conducted to determine the surface dose of the FFF photon beams. The measurement from each

detector showed that the surface dose increased with increasing field size above 2 cm × 2 cm, whereas for decreasing field sizes below 2 cm × 2 cm, the surface dose increased. These results are consistent with those of previous studies using radiochromic films, ionization chambers, and diodes (Bilge et al., 2010; Chen et al., 2010). The energy spectrum, electron contamination from collimator assembly and air, and lateral scattering falling off in FFF photon beams are the reasons behind the variations in the surface doses with field sizes (Apipunyasopon et al., 2013, Yokoyama et al., 2004). It can be seen from Figure 3.19 that for small field sizes of 0.6 cm × 0.6 cm to 6 cm × 6 cm, the SNC125c showed the highest value for D_S, whereas the lowest value was obtained with the EBT3. The maximum variation in D_S was 38.93% between SNC125c and EBT3 for the smallest field sizes ≤ 1 cm × 1 cm. Comparison of D_S between PinPoint and SNC125c showed that the variation was within 3% for all field sizes except 0.6 cm× 0.6 cm (3.57%). The difference in D_S between PinPoint and EDGE was less than 8% for all field sizes. These results are in agreement with earlier comparisons carried out between ionization chambers and diodes (Bucciolini et al., 2003; Djouguela et al., 2008). The over-response of surface dose values measured using ionization chambers and diodes have been reported in an earlier study (Chen et al., 2010). The values obtained by the EBT3 were the lowest for all field sizes when compared with those obtained with other detectors used in this study. These measured values were as per those reported in previous studies (Morales et al., 2014; Wang et al., 2012). Radiochromic films may be ideal for the measurement of doses in high-dose gradient regions, such as build-up or surface dose regions, owing to their high spatial resolution and low spectral sensitivity.

The PDD measured with the SNC125c had the highest value after renormalization to the peak value than with other dosimeters. The under-responses of PDD data points at shallow depths were due to the perturbation, while volume effects resulted in over-responses at deeper depths. Similar results have been reported earlier (Akino et al., 2020). The PDD of the 6 MV FFF beam was found to correspond to that of a standard 4–5 MV FF beam. Detector to detector variation of D_{10} for 0.6 cm × 0.6 cm field size was noticeable (RSD = 1.80%), whereas other field sizes showed negligible deviation (RSD ≤ 0.62). D_{10} measured with SNC125c showed the largest variations of 3.38% for field size 0.6 cm × 0.6 cm when compared with that of EBT3. This deviation is due to the volume averaging effect in the SNC125c. Additionally,

the positional accuracy of the detector with the central axis is important in PDD measurement as 1 mm of deviation from the central axis for a 1 cm × 1 cm field results in a 2% error in PDD measurement (Zefkili et al., 1994). D_{10} values measured using EBT3, PinPoint, and EDGE were found to be in good agreement for all the small field sizes measured in this study.

Generally, the depth of the maximum dose depends on the beam quality and field size. All the detectors showed that depth of maximum dose increased gradually from field size of 0.6 cm × 0.6 cm and attained a saturation value from 3 cm × 3 cm field size onwards, expect SNC125c, which showed a saturated value from 2 cm × 2 cm filed size onwards. The ranges of the minimum and maximum values of d_{max} recorded with various detectors were 12.0–12.1 mm and 15.0–15.2 mm respectively. The decrease in d_{max} values for those below 3 cm × 3 cm field size is due to the lack of secondary electron equilibrium in smaller field definitions (Wuerfel, 2013).

3.5 CONCLUSIONS

In the present study, the characteristic parameters of small-fields of 6 MV FFF photon were measured using an SNC125c, PinPoint, EBT3, TLD-100, and EDGE. The study found that the PinPoint, EBT3, TLD-100, and EDGE appear to be the detectors of choice for small field output factor measurement of a 6 MV FFF beam; however, the PinPoint should be used carefully for the smallest field size (0.6 cm × 0.6 cm), as it requires a correction that is slightly higher than 10% (Azangwe et al., 2014). The EDGE must be calibrated against the ion chamber when used for the output factor measurement. EDGE and EBT3 are optimal for measuring beam profile. The EBT3, PinPoint, and EDGE can be selected for the percentage depth dose measurement. The EBT3 appears suitable for surface dose estimation, whereas measurements obtained from ionization chambers and diodes require an appropriate correction factor for the over-response of surface doses. In summary, this study describes the detector suitable for the measurement of a particular dosimetric parameter of a 6 MV FFF small photon beam.